This is an open access article published under an ACS AuthorChoice License, which permits copying and redistribution of the article or any adaptations for non-commercial purposes.

ACS OMEGA

http://pubs.acs.org/journal/acsodf

Article

Designing Novel Zn-Decorated Inorganic $B_{12}P_{12}$ Nanoclusters with Promising Electronic Properties: A Step Forward toward Efficient CO_2 Sensing Materials

Shahid Hussain, Shahzad Ali Shahid Chatha, Abdullah Ijaz Hussain, Riaz Hussain, Muhammad Yasir Mehboob, Tahsin Gulzar, Asim Mansha, Nabeel Shahzad, and Khurshid Ayub*

Cite This: *ACS Omega* 2020, 5, 15547−15556

Read Online

ACCESS | Metrics & More | Article Recommendations | Supporting Information

ABSTRACT: Gas sensing materials have been widely explored recently owing to their versatile environmental and agriculture monitoring applications. The present study advocates the electronic response of Zn-decorated inorganic $B_{12}P_{12}$ nanoclusters to CO_2 gas. Herein, a series of systems CO_2−Zn−$B_{12}P_{12}$ (**E1**−**E4**) are designed by adsorption of CO_2 on Zn-decorated $B_{12}P_{12}$ nanoclusters, and their electronic properties are explored by density functional theory. Initially, placement of Zn on $B_{12}P_{12}$ delivers four geometries named as **D1**−**D4**, with adsorption energy values of −57.12, −22.94, −21.03, and −14.07 kJ/mol, respectively, and CO_2 adsorption on a pure $B_{12}P_{12}$ nanocage delivers one geometry with an adsorption energy of −4.88 kJ/mol. However, the interaction of CO_2 with **D1**−**D4** systems confers four geometries named as **E1** (E_{ad} = −75.12 kJ/mol), **E2** (E_{ad} = −25.89 kJ/mol), **E3** (E_{ad} = −42.43 kJ/mol), and **E4** (E_{ad} = −28.73 kJ/mol). Various electronic parameters such as dipole moment, molecular electrostatic potential analysis, frontier molecular orbital analysis, Q_{NBO}, global descriptor of reactivity, and density of states are also estimated in order to understand the unique interaction mechanism. The results of these analyses suggested that Zn decoration on $B_{12}P_{12}$ significantly favors CO_2 gas adsorption, and a maximum charge separation is also noted when CO_2 is adsorbed on the Zn−$B_{12}P_{12}$ nanocages. Therefore, the Zn-decorated $B_{12}P_{12}$ nanocages are considered as potential candidates for application in CO_2 sensors.

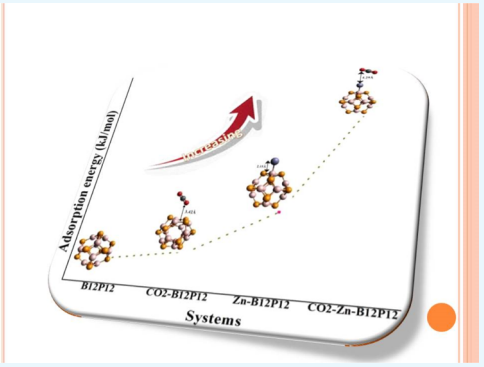

1. INTRODUCTION

Nanoscience has developed a revolutionary trend in various fields of science. Functional nanomaterials are now attracting the modern research community because of their distinct structural and electronic properties.[1,2] Recently, nanostructure semiconductors have gained significant interest from the scientific community because of their distinct physical and chemical properties.[2−4] Nanostructures such as fullerenes, nanotubes, and nanoclusters have also received great interest for many applications such as catalysis, biotechnology, gas sensors, and cluster protection.[5−7]

Nanomaterials also find applications in transistors and adsorption because of their high surface/volume ratio. Metals adsorbed on the surface of nanocages enhance catalytic and adsorption properties.[8−10] Group III−V semiconductors have gained importance because of their extensive use in light-emitting diodes, nonlinear optics,[11−13] and in microelectronic devices.[14−16] These are also used as adsorbents/sensors for various analytes. The small-sized solid-state adsorbents can easily be synthesized at low cost. These are also reproducible, which makes them excellent candidates for sensor applications.[17]

Adsorption of gases on nanostructures, nanocages, and nanotubes are part of valuable literature. For example, Ahmadi et al. studied the adsorption energies of nitrogen oxide and carbon monoxide on MgO nanotubes.[18] In addition, different reports specifically on the adsorption properties of different molecules on the surface of $(AlP)_x$, $(AlN)_x$, $(BP)_x$, and $(BN)_x$ nanocages are also part of valuable literature. For example, Ayub[19] studied the binding affinity of helium and neon atoms with $X_{12}Y_{12}$ (X = B, Al, and Y = N, P) in exohedral and endohedral modes. Similarly, Rad et al.[20] demonstrated the ability of $Al_{12}N_{12}$ nanoclusters for adsorption of BCl_3 by using density functional theory calculations. In another report, Rad and Ayub[21] studied the geometries and electronic properties of Ni-doped $Al_{12}N_{12}$ nanocages. Baei et al. showed $B_{12}N_{12}$ nanoclusters as an outstanding adsorbent for aniline from groundwater to tackle the environmental issues.[22] Soltani et al. studied phenol interactions with various nanocages through density functional theory (DFT) calculations.[10] Significant

Received: April 13, 2020
Accepted: June 5, 2020
Published: June 19, 2020

ACS Publications

© 2020 American Chemical Society

literature is available for adsorption of various molecules such as pyridine,[23] methylamine,[24] hydrogen cyanide,[25] and fluorine[26] on $B_{12}N_{12}$ nanocages. Adsorption of biological molecules such as nitrogenous basis (uracil, cytosine, and adenine)[27] and guanine[28] on these nanocages are also part of valuable literature. In valuable literature, report on adsorption of pyrrole on $Al_{12}N_{12}$, $Al_{12}P_{12}$, $B_{12}P_{12}$, and $B_{12}N_{12}$ nanocages is also present.[9] Rad et al. studied the effective adsorption of O_3 on $B_{12}P_{12}$, $Al_{12}N_{12}$, and $B_{12}N_{12}$ nanocages previously.[29] Similarly, $B_{12}P_{12}$ nanocages were also utilized for hydrogen gas adsorption.[30]

Recently, metal decorations (dopants) have been launched to improve the adsorption, electronic,[31−35] and nonlinear optical properties of nanostructures.[36,37] Zhang et al.[38] carried out DFT calculations to examine the hydrogen adsorption on pure and nickel metal-decorated aluminum nitride nanocages. They studied that in a pure AlN nanocage, a single Al atom avails only one H_2, whereas the nickel atom in Ni−AlN has a tendency to adsorb three hydrogen molecules. Ayub et al. studied that nickel decoration on $B_{12}N_{12}$[39] and $B_{12}P_{12}$[30] significantly enhanced the adsorption of hydrogen gas. Nickel metal decoration on $(XY)_{12}$ was also proved useful for adsorption of SO_2[40] and acetylene.[41] Similarly, Shakerzadeh et al. investigated adsorption of phosgene gas on Al- and Ga-doped $B_{12}N_{12}$ and $B_{16}N_{16}$ nanoclusters.[42] Decoration of metal is useful in order to enhance the effective role of these nanocages in NLO materials.[43,44] In addition, these nanocages exhibit a variety of applications such as field-effective transistors,[45] storage devices,[46] and magnetic nanoparticles.[47]

Because of the rapid increase in industrialization, population, and traffic, the percentage of CO_2 also increases in the atmosphere as a result of fossil fuel burning. Ultimately, the greenhouse effect is increasing and making the earth warmer. Oceans act as a sink of CO_2 and the dissolution of CO_2 affecting the system by lowering the pH. Therefore, it is important to monitor and control this pollutant to make the environment more safe and friendly. Recently, the research is devoted to develop some gas sensors for monitoring hazardous gas for its optimum level.[48−50]

Carbon sequestration is a process through which atmospheric freely available carbon dioxide (CO_2) is captured and stored through a natural process, so it has become a most important feature in environment protection. For better results, the sequestration material should be of large surface area for effective absorption and easy accessibility to atmospheric carbon dioxide.[51,52] Therefore, it is important to capture this dangerous gas from the environment in order to make the environment green and clean. Recently, Cu-decorated $B_{12}N_{12}$ has been used to detect the harmful phosgene gas.[53] Similarly, Hussain et al. explored the remarkable response of Zn-doped $B_{12}P_{12}$ to SO_2 gas.[54]

In the literature, there is no detailed report on the adsorption of carbon dioxide on Zn-decorated nanocages. Analysis is performed for all promising relaxed structures of CO_2-adsorbed nanocages on the above-mentioned surfaces. We discuss the result on adsorption through the net charge transfer, values of binding energy, molecular electrostatic potential (MEP) analysis, dipole moment, density of states (DOS), global descriptor of energy, and the highest occupied molecular orbital (HOMO) and the lowest unoccupied molecular orbital (LUMO) distribution on all possible forms of $B_{12}P_{12}$ nanocages. Finally, we recommend a kind of novel systems with promising electronic properties for CO_2 sensing materials.

2. RESULTS AND DISCUSSION

The relaxed geometry of a $B_{12}P_{12}$ nanocage at the B3LYP method with the 6-31G(d,p) level of DFT is shown in Figure 1. Two types of rings are present in the $B_{12}P_{12}$ nanocage, one is

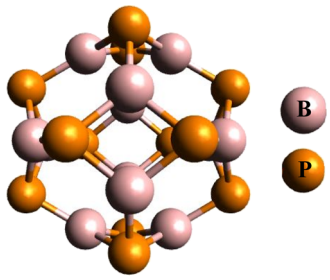

Figure 1. $B_{12}P_{12}$ DFT-based relaxed structure with the aid of the B3LYP method along with the 6-31G(d,p) level of DFT.

tetragonal and the other is hexagonal. Both rings are interconnected in order to gain a three-dimensional nanocage. Similarly, two types of bonds are present in $B_{12}P_{12}$, one is b_{64} (bond shared between tetragonal and hexagonal ring) and the other is b_{66} (bond shared between two hexagonal rings). In an optimized geometry of $B_{12}P_{12}$ nanocage, the b_{64} and b_{66} bond lengths are 1.93 and 1.91 Å, respectively.

2.1. Interaction Energies along with Bond Lengths.

Pure $B_{12}P_{12}$ has equal number of electropositive and electronegative atoms. Six different sites are present for the decoration of a late transition metal (Zn). These sites are named as: (i) b_{66} [decoration of Zn on a common bond present between two six-member (hexagonal) rings], (ii) b_{64} [placement of Zn metal specifically on a bond shared between one four-member (tetragonal) and one six-member (hexagonal) ring], (iii) B_{top} (Zn metal installed on boron top), (iv) P_{top} (positing of Zn metal on phosphorus top), (v) r_6 (bringing Zn metal on the top center of the hexagonal ring), and (vi) r_4 (putting Zn metal on top of the tetragonal ring). We tried all the above-mentioned positions, but only four geometries could be optimized because some initial input geometries switched to other geometries. The obtained geometries are named as **D1** (Zn@b_{64}), **D2** (Zn@B_{top}), **D3** (Zn@r_4), and **D4** (Zn@P_{top}). In the **D1** geometry, the positioning of the late transition metal (Zn) elongates the B−P bond length to 3.66 Å (as compared to 1.93 Å in pure BP) with an interaction energy value of −57.12 kJ/mol. In the **D2** geometry, the decoration of Zn metal on $B_{12}P_{12}$ does not bring much change in the B−P bond length (bond length$_{(B-P)}$ = 1.98 Å), and the interaction energy value in this case is −22.94 kJ/mol. In the **D3** and **D4** geometries, the interaction of Zn metal with the $B_{12}P_{12}$ nanocage executes a negligible alteration in the B−P bond length with interaction energy values of −21.03 and −14.07 kJ/mol, respectively. Similarly, the distances of Zn metal from the $B_{12}P_{12}$ nanocage in **D1**, **D2**, **D3**, and **D4** geometries are 2.15, 2.15, 2.96, and 3.00 Å, respectively, as shown in Figure 2. From the preceding discussion, it is cleared that **D1** is the most stable and **D4** is the least stable geometry among **D1**−**D4**. This might be due to the shape of the geometries; that is, in **D1**, adsorption of Zn metal changes the normal shape of $B_{12}P_{12}$ to an open envelop shape, which ultimately reduces the strain of the tetragonal ring and becomes stable, whereas in

https://dx.doi.org/10.1021/acsomega.0c01686
ACS Omega 2020, 5, 15547−15556

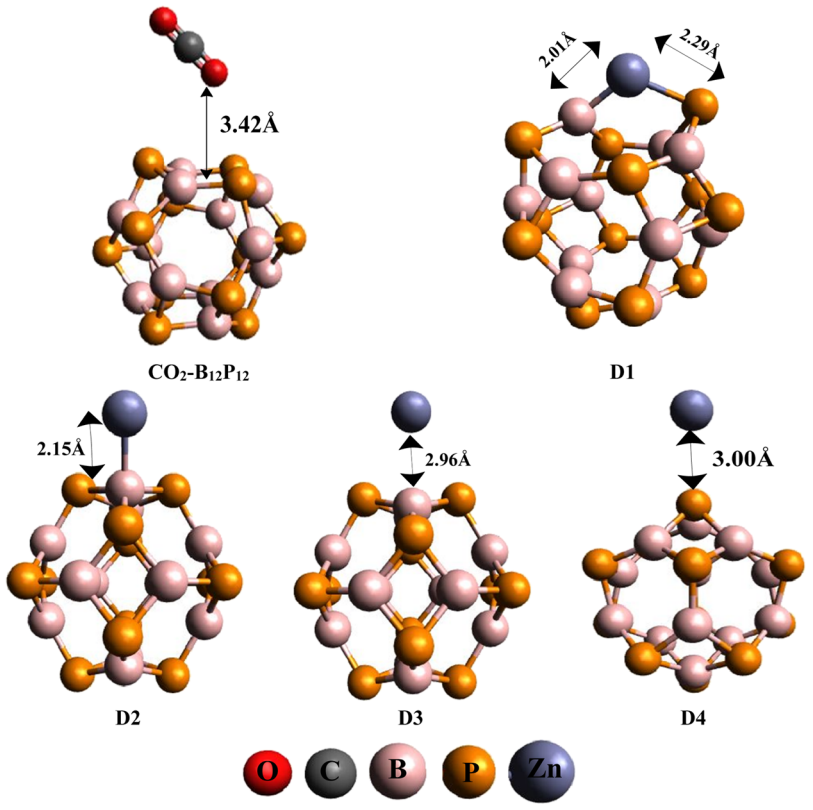

Figure 2. Optimized geometries of CO_2−$B_{12}P_{12}$ and **D1**−**D4** systems.

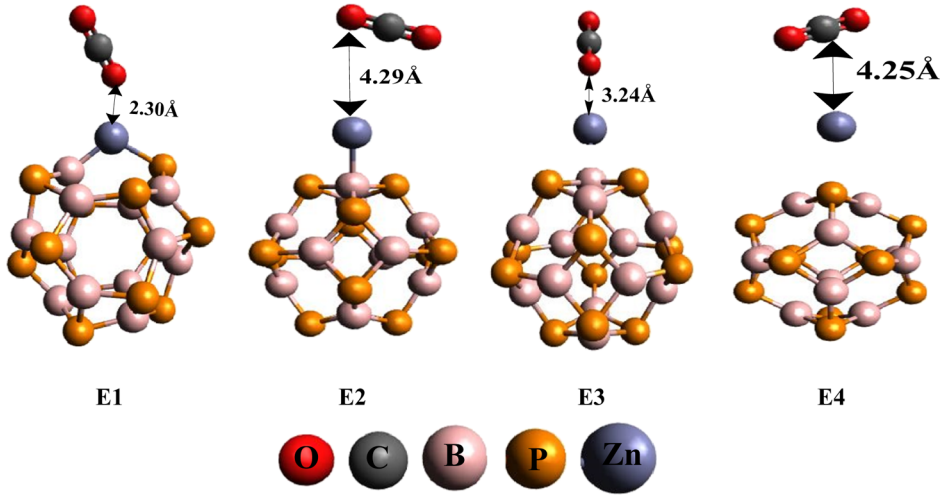

Figure 3. Optimized geometries of CO_2-adsorbed Zn−$B_{12}P_{12}$ (**E1**−**E4**) systems.

D4, $B_{12}P_{12}$ does not provide enough room for adsorption of Zn metal, which decreases the stability of the Zn-doped system. Apart from this, the distance of Zn metal from the BP nanocage is very crucial, which suggests that large distance of Zn from BP in **D4** causes weak adsorption and vice versa.

Further, adsorption of CO_2 gas on pure and Zn-doped $B_{12}P_{12}$ nanocages is being analyzed. CO_2 absorption on bare $B_{12}P_{12}$ exhibits the physisorption phenomenon. The large distance of gas from the nanocage (d_{CO_2-BP} = 3.42 Å) and the low adsorption value (E_d = −4.88 kJ/mol) indicated that CO_2 is not favorably adsorbed on bare $B_{12}P_{12}$. Besides this, CO_2 is also adsorbed on Zn-doped $B_{12}P_{12}$ nanocages (**D1**−**D4**), which deliver four geometries named as **E1**, **E2**, **E3**, and **E4**. We gained **E1**−**E4** after CO_2 adsorption on **D1**−**D4**, respectively, as shown in Figure 3. The adsorption energy values in **E1** (E_{ad} = −75.12 kJ/mol), **E2** (E_{ad} = −25.89 kJ/mol), **E3** (E_{ad} = −42.43 kJ/mol), and **E4** (E_{ad} = −28.73 kJ/mol) suggest that CO_2 gas is favorably adsorbed on Zn-doped systems, which suggested potential utilization of these materials for CO_2 gas sensing as compared to pure $B_{12}P_{12}$. In all geometries (**E1**−**E4**), orientation of CO_2 on Zn-decorated BP is different (Figure 3). Different orientations display different distances from the Zn−BP system. Among **E1**−**E4**, **E1** and **E3** disclosed high adsorption energy values, and these are due to the small distance of CO_2 from the Zn−$B_{12}P_{12}$ nanocage [$d_{CO_2-Zn-BP}$ (**E1** = 2.30 Å and **E3** = 3.24 Å)]

https://dx.doi.org/10.1021/acsomega.0c01686
ACS Omega 2020, 5, 15547−15556

Table 1. Distance of Zn Metal from the $B_{12}P_{12}$ Nanocage (Å), Distance between the Closest Atom of CO_2 and Zn Metal (Å), Natural Bonding Orbital Charge (Q_{NBO}) on Metal and Gas (eV), Dipole Moment (Debye), and Adsorption Energy of All Systems (kJ/mol)

systems	d_{Zn-BP} (Å)	d_{CO_2-Zn}(Å)[a]	Q_{NBO} on CO_2 (eV)	Q_{NBO} on Zn (eV)	μ_D (D)	E_{ad}[b] (kJ/mol)
$B_{12}P_{12}$					0.00	
$B_{12}P_{12}-CO_2$			−0.624		0.33	−4.88
Zn−BP (**D1**)	2.15			1.937	2.25	−57.12
Zn−BP−CO_2 (**E1**)		2.30	−0.692		5.36	−75.12
Zn−BP (**D2**)	2.15			0.524	3.24	−22.94
Zn−BP−CO_2 (**E2**)		4.25	−0.677		3.07	−25.89
Zn−BP (**D3**)	2.96			0.076	0.94	−21.03
Zn−BP−CO_2 (**E3**)		3.24	−0.685		3.00	−42.43
Zn−BP (**D4**)	3.00			−0.422	0.61	−14.07
Zn−BP−CO_2 (**E4**)		4.25	−0.681		3.30	−28.73

[a]Distance between the nearest CO_2 atom from the Zn metal. [b]Adsorption energies of different systems.

as shown in Table 1. The closest distance of CO_2 from Zn−$B_{12}P_{12}$ with high adsorption energy is found in the case of **E1**, where Zn metal effectively offers better adsorption because of the small distance of Zn from the $B_{12}P_{12}$ nanocage. Therefore, small distance allows favorable adsorption of CO_2 on Zn-doped $B_{12}P_{12}$ nanocages. From the above discussion, it is concluded that adsorption of late transition metal (Zn) brings some structural changes in the $B_{12}P_{12}$ nanocage, which significantly enhance the adsorption rate of CO_2 gas.

The literature is quite extensive on the utilization of different surfaces for CO_2 detection and adsorption. We have now given comparison of our results with those available in the literature on different nanoclusters. Moreover, in valuable literature, reports related to CO_2 adsorption on different nanocages are present. Baei et al.[5] studied different orientations of CO_2 on $B_{12}N_{12}$ nanocages with adsorption energies ranging from −14.99 to −15.45 kcal/mol. Similarly, Kauffman et al.[55] studied the interaction of CO_2 with the Au_{25} cluster with an adsorption energy value of 0.13 eV. Liang et al.[56] studied the physisorption of CO_2 on $B_{12}N_{12}$, Li@$B_{12}N_{12}$, Na@$B_{12}N_{12}$, and K@$B_{12}N_{12}$ with adsorption energies of −1.86, −2.96, −3.18, and −2.66 kcal/mol, respectively. Based on DFT study, Jiang et al.[57] reported that $Al_{11}Mg_3^-$ nanoclusters had excellent capturing capacity of CO_2 (E_{ad} = 0.114 eV). Guo et al.[58] reported the adsorption of CO_2 on a hexagonal BN sheet, where the adsorption energies are as high as 0.42 eV (parallel orientation of CO_2 on the h-BN sheet) and 0.44 eV (vertical orientation of CO_2 on the h-BN sheet). The adsorption energies of Zn-doped boron phosphide nanocages (in our case) are much higher (−6.18 to −17.96 kcal/mol) than the reported values of adsorption energies of CO_2 on different surfaces. These results illustrate the efficiency and potential of the Zn−$B_{12}P_{12}$ nanocluster for CO_2 adsorption.

2.2. Dipole Moment. Dipole moment is another tool to explore the electronic change in the $B_{12}P_{12}$ nanocluster upon Zn decoration and CO_2 adsorption. As we know, the electropositive and electronegative atoms are equal in number; therefore, a pure $B_{12}P_{12}$ nanocage is a symmetrical structure with zero dipole moment. However, decoration with late transition metal such as Zn brings significant change in the dipole moment as shown in Table 1. The dipole moments in **D1**−**D4** geometries are noted as 2.25, 3.24, 0.94, and 0.61 D, respectively. All values of dipole moments revealed that the placement of Zn significantly disturbs the charge separation in the $B_{12}P_{12}$ nanocage. The disturbance in charge separation is high in the case of **D1** and **D2** systems, which might be due to the small distance of Zn from BP. In addition, the disturbance in charge separation of $B_{12}P_{12}$ is also analyzed in $CO_2-B_{12}P_{12}$ and **E1**−**E4** geometries. Initially, when carbon dioxide is placed on top of $B_{12}P_{12}$, the dipole moment value is quite small (0.33 D), which indicates that adsorption of CO_2 does not bring significant change in charge separation. However, when CO_2 is positioned on Zn-decorated $B_{12}P_{12}$ nanocages (**E1**−**E4**), significant changes in the dipole moment value are noted. The dipole moment values for **E1**−**E4** are 5.36, 3.07, 3.00, and 3.30 D, respectively. These values suggest that CO_2 adsorption on **D1**−**D4** geometries significantly affects the charge separation with dipole moment values as compared to the rest of the geometries. Large adsorption energies cause high charge separation (large dipole moment value) in **E1**−**E4**. The decreasing order of the dipole moment for all systems is **E1** > **E4** > **D2** > **E2** > **E3** > **D1** > **D3** > **D4** > $CO_2-B_{12}P_{12}$. From the preceding discussion, it is cleared that CO_2 adsorption on Zn-decorated $B_{12}P_{12}$ nanocages enhanced charge separation of $B_{12}P_{12}$ with large values of dipole moment.

2.3. Q_{NBO}. In support of dipole moment, Q_{NBO} analysis is performed in order to understand the strong interaction of Zn and CO_2 with the $B_{12}P_{12}$ nanocage. In the case of **D1**−**D4** geometries, the increase in Q_{NBO} is consistent with the increase in the dipole moment value. A highest Q_{NBO} value is noted in the **D1** system with large dipole moment and E_{ad}. The decreasing order of Q_{NBO} for **D1**−**D4** is **D1** > **D2** > **D3** > **D4**. This trend is consistent with the dipole moment trend of **D1**−**D4** geometries. However, the Q_{NBO} analysis in CO_2-adsorbed Zn-doped $B_{12}P_{12}$ systems (**E1**−**E4**) exhibited negative values. This might be due to shifting of charge from Zn−BP, which makes CO_2 slightly negative in nature (Table 1). Therefore, from Q_{NBO} discussion, it is illustrated that Zn decoration on $B_{12}P_{12}$ nanocages shows a consistent trend with dipole moment, and CO_2 adsorption on these metal-decorated $B_{12}P_{12}$ nanocages makes carbon dioxide slightly negative in nature.

2.4. MEP Analysis. MEP analysis is another useful parameter to explore the extent of charge separation within a molecule. MEP analysis also correlates the geometry of a system with physiochemical properties such as dipole moment, chemical reactivity, and partial charges. MEP analysis is estimated at the B3LYP/6-31G(d,p) level of DFT. Figure 4 discloses the charge separation. Generally, blue area represents the electropositive end (boron in the present case), yellow area specifies the electronegative end (phosphorus in the present case), while green area represents the mean potential (the area

https://dx.doi.org/10.1021/acsomega.0c01686
ACS Omega 2020, 5, 15547−15556

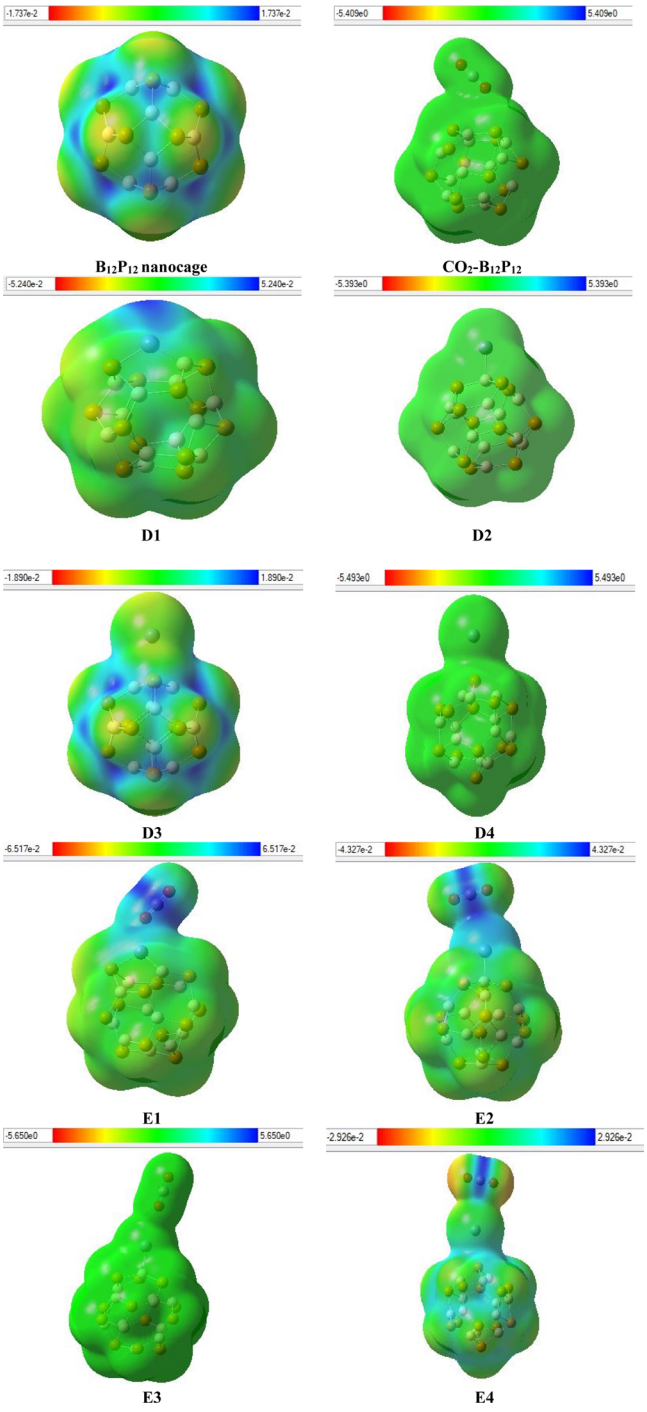

Figure 4. MEP of all systems (for understanding the colors in these figures, the reader must read the web version of this article). The isosurface value is 0.02e/Å^3.

between the two extremes) in web version. Pure $B_{12}P_{12}$ being symmetrical shows equal charges. Fixing of CO_2 on pure $B_{12}P_{12}$ does not bring significant charge separation as shown in Figure 4. However, placement of Zn on pure nanocage causes positive charge shifting on top of the Zn metal (blue color) because of the electropositive nature of late transition metal and the yellow area in the nanocage becomes less intense. However, in the case of **E1**−**E4**, major charge separation occurs as the blue area is shifted to Zn metal and the carbon center of CO_2 while both oxygen atoms of CO_2 exhibit extreme negative charge. All this charge shifting is attributed to an increase in dipole moment (D). For instance, pure $B_{12}P_{12}$ has zero dipole moment, whereas Zn-decorated $B_{12}P_{12}$ has some value of dipole moment.

Next, the correlation of the distribution of charges (in MEP) with the dipole moment is explored. In **D1**−**D4** systems, an irregular trend of dipole moment is observed. A maximum dipole moment is noted in the **D2** geometry; however, this value does not bring much change in the electrostatic potential plot, probably because of the large distance of metal and B-top adsorption of metal on BP. The second largest dipole moment value is obtained in the **D1** geometry. In **D1**, some charge density is shifted toward the metal end upon Zn adsorption on BP, probably because of the incorporation of metal with the bond present between the tetragonal and hexagonal ring. The electrostatic potential plots of geometries **D3** and **D4** also exhibit a similar potential. Again, this is probably due to large distances and low values of dipole moment along with low adsorption energies values, which do not bring any change in charge distribution. Overall, the electrostatic potential (ESP) of **D1**−**D4** is different from each other because of the difference in dipole moment values and orientation along with the distance of metal from the cage.

2.5. Electronic Properties. The frontier molecular orbitals (FMOs) (energies of HOMOs and LUMOs), Fermi level, and the HOMO−LUMO gap of systems are observed at the B3LYP/6-31G(d,p) level of density functional theory. The results of these key parameters are tabulated in Table 2. Pure

Table 2. Energies of HOMO, LUMO, and Fermi Level (E_{FL}) along with the HOMO−LUMO Energy Gap (E_g) in eV of All Systems

system	E_{HOMO} (eV)	E_{FL} (eV)	E_{LUMO} (eV)	E_g (eV)
$B_{12}P_{12}$	−6.83	−4.98	−3.13	3.70
$B_{12}P_{12}$−CO_2	−6.81	−4.96	−3.11	3.69
Zn−BP (**D1**)	−5.92	−4.45	−2.97	2.95
Zn−BP−CO_2 (**E1**)	−5.64	−4.21	−2.77	2.88
Zn−BP (**D2**)	−6.25	−4.71	−3.16	3.09
Zn−BP−CO_2 (**E2**)	−6.27	−4.73	−3.19	3.08
Zn−BP (**D3**)	−5.63	−4.41	−3.19	2.43
Zn−BP−CO_2 (**E3**)	−6.16	−4.59	−3.02	3.41
Zn−BP (**D4**)	−5.57	−4.37	−3.17	2.40
Zn−BP−CO_2 (**E4**)	−5.61	−4.40	−3.19	2.42

$B_{12}P_{12}$ is viewed as semiconductor, which holds a HOMO−LUMO gap of 3.70 eV. The HOMO and LUMO orbitals of $B_{12}P_{12}$ are located at −6.83 and −3.13 eV, respectively. Generally, the Fermi level (E_{FL}) of a molecule is observed at the midpoint of the HOMO−LUMO gap.[59] The Fermi level is found at −4.98 eV for the $B_{12}P_{12}$ nanocage. When Zn is installed on the $B_{12}P_{12}$ nanocage (**D1**−**D4**), a remarkable change in the energies of HOMO and LUMO is observed. The energies of HOMO for **D1**−**D4** are −5.92, −6.25, −5.63, and −5.57 eV, whereas the energies of LUMO are −2.97, −3.16, −3.19, and −3.17 eV, respectively. In all Zn-doped BP systems (**D1**−**D4**), the energies of HOMO are increased, whereas the LUMO energies are decreased, which ultimately causes narrowing of the HOMO−LUMO gap. The HOMO−LUMO gap (E_g) is related to the conductivity of a material,[60,61] and this direct relation is commonly measured with the aid of the following equation

$$\sigma\alpha \exp(-E_g/KT) \quad (1)$$

https://dx.doi.org/10.1021/acsomega.0c01686
ACS Omega 2020, 5, 15547−15556

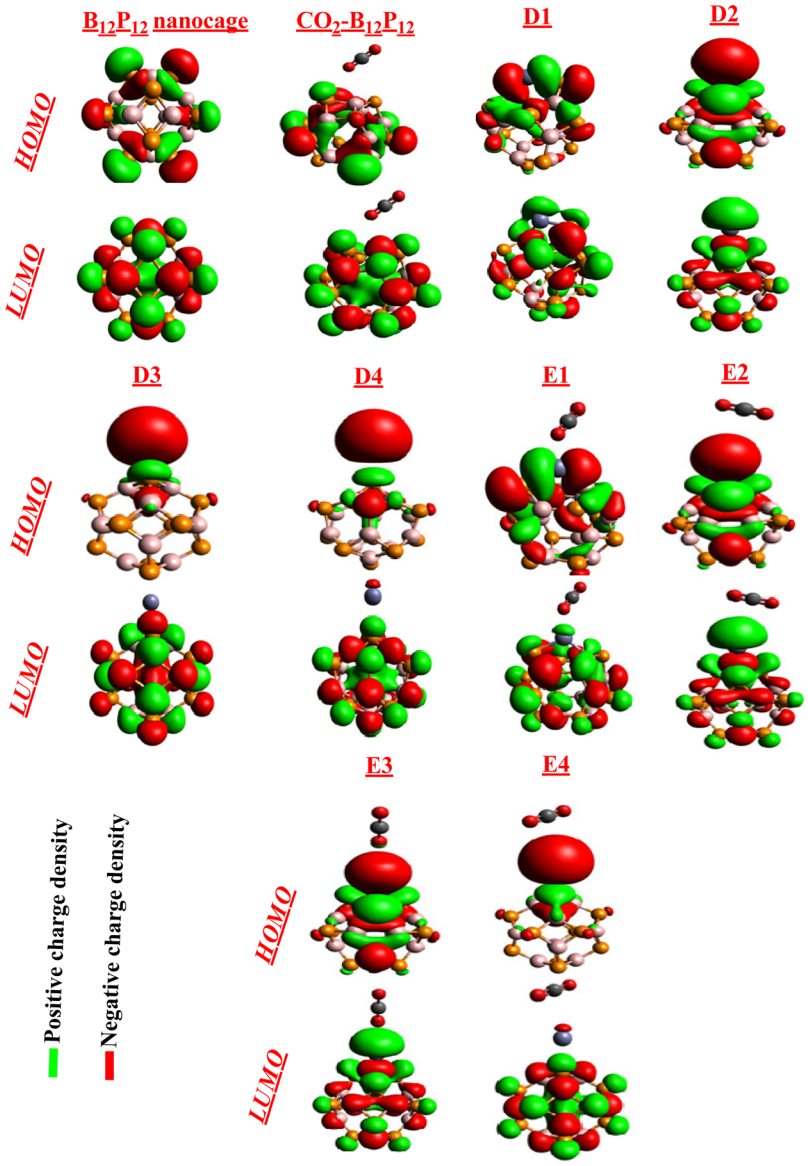

Figure 5. Side views of HOMO and LUMO of different systems. The isosurface value is 0.02e/Å^3.

The widths of H−L gaps for **D1**−**D4** are 2.95, 3.09, 2.43, and 2.40 eV, respectively. These values disclosed the great conductivity of Zn-decorated $B_{12}P_{12}$ nanocages. When CO_2 is adsorbed on pure $B_{12}P_{12}$, no such sifting of HOMO and LUMO orbital is observed. The difference in the energy gap of pure and CO_2−$B_{12}P_{12}$ is very minute as shown in Table 2. However, adsorption of CO_2 on Zn-decorated $B_{12}P_{12}$ nanocages (**E1**−**E4**) appreciably destabilizes the HOMO orbitals and stabilizes the LUMO orbitals. The HOMO energies of **E1**−**E4** geometries are −4.21, −4.73, −4.59, and −4.40 eV, whereas the LUMO energies are −2.77, −3.19, −3.02, and −3.19 eV, respectively. All these values indicated destabilization of HOMO orbital and stabilization of LUMO orbital (after CO_2 adsorption on **D1**−**D4**), which results in narrowing of the HOMO−LUMO energy gap. The HOMO−LUMO energy gap upon Zn decoration on $B_{12}P_{12}$ decreases from 3.70 to 2.95 (**D1**), 3.09 (**D2**), 2.43 (**D3**), and 2.40 (**D4**). Therefore, Zn decoration significantly causes narrowing of the HOMO−LUMO energy gap with high conductivity as compared to pure and CO_2−$B_{12}P_{12}$ nanocages. The HOMO−LUMO energy gaps of **E1**−**E4** are 2.88, 3.08, 3.41, and 2.42 eV, respectively. The values of HOMO−LUMO energy gap show that CO_2 adsorption on **D1**−**D4** significantly reduces the HOMO−LUMO energy gap as compared to pure and CO_2−$B_{12}P_{12}$, which suggest that Zn metal decoration favors CO_2 adsorption. However, the Fermi levels for **E1**−**E4** are noted at −4.21, −4.73, −4.59, and −4.40 eV, respectively. The decreasing order of HOMO−LUMO energy gap for all systems including the pure $B_{12}P_{12}$ nanocage is $B_{12}P_{12}$ > CO_2−$B_{12}P_{12}$ > **E3** > **D2** > **E2** > **D1** > **E1** > **D3** > **E4** > **D4**. From this trend and the above-mentioned discussion, it is noted that Zn decoration on $B_{12}P_{12}$ significantly enhances the conductivity of the $B_{12}P_{12}$ nanocage, and Zn decoration also makes the BP nanocage an efficient material for CO_2 adsorption (Figure 5).

The distribution of HOMO and LUMO densities on all systems at B3LYP in conjunction with the 6-31G(d,p) level of DFT is shown in Figure 6.

Generally, DOS is performed in support of FMOs. The DOS graphs are shown in Figure 6, which reveal that the HOMO and LUMO densities are equally shared within the whole $B_{12}P_{12}$ nanocage. However, placement of Zn on $B_{12}P_{12}$ shifted the HOMO and LUMO toward the Zn center in the **D1** and

https://dx.doi.org/10.1021/acsomega.0c01686
ACS Omega 2020, 5, 15547−15556

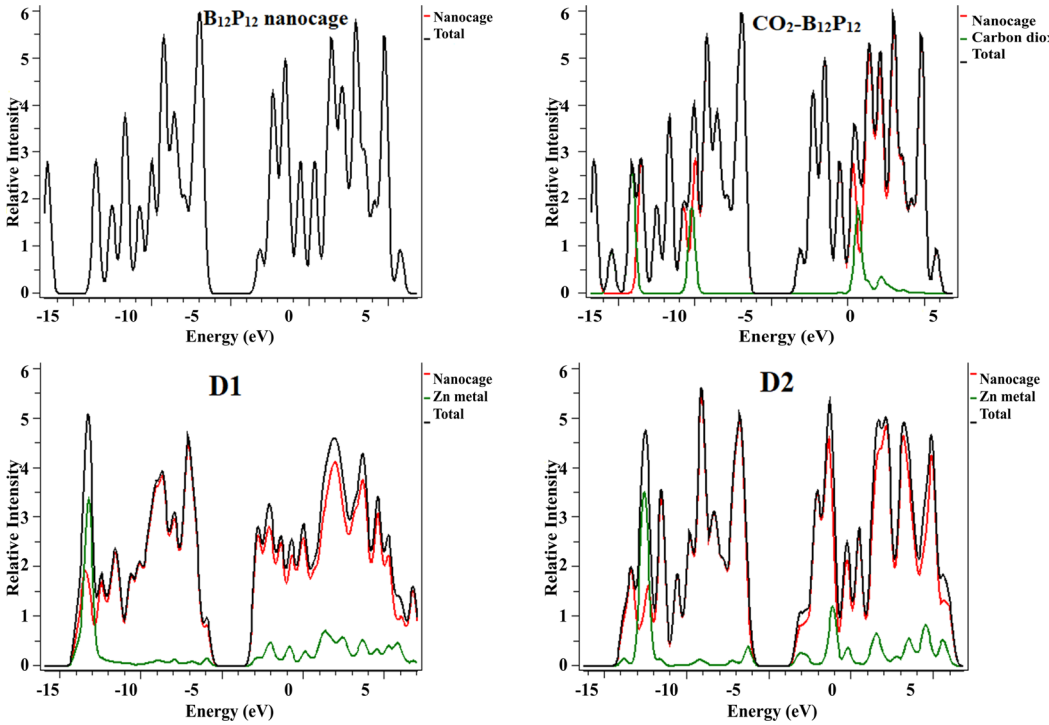

Figure 6. DOS for all systems at the B3LYP/6-31G(d,p) level of DFT.

Table 3. IP, EA, X (Electronegativity), μ (Chemical Potential), η (Global Hardness), S (Global Softness), and ω (Global Electrophilicity) of All Systems

system	IP (eV)	EA (eV)	X (eV)	μ (eV)	H (eV)	S (eV^{-1})	Ω (eV)
BP	6.830	3.130	4.980	−4.980	1.850	0.270	6.703
BP−CO_2	6.810	3.110	4.960	−4.960	1.850	0.270	6.649
Zn−BP (**D1**)	5.920	2.970	4.445	−4.445	1.475	0.339	6.698
Zn−BP−CO_2 (**E1**)	5.640	2.770	4.205	−4.205	1.435	0.348	6.161
Zn−BP (**D2**)	6.250	3.160	4.705	−4.705	1.545	0.324	7.164
Zn−BP−CO_2 (**E2**)	6.270	3.190	4.730	−4.730	1.540	0.325	7.264
Zn−BP (**D3**)	5.630	3.190	4.410	−4.410	1.220	0.410	7.971
Zn−BP−CO_2 (**E3**)	6.160	3.020	4.590	−4.590	1.570	0.318	6.710
Zn−BP (**D4**)	5.570	3.170	4.370	−4.370	1.200	0.417	7.957
Zn−BP−CO_2 (**E4**)	5.610	3.190	4.400	−4.400	1.210	0.413	8.000

D2 geometries. However, in the case of **D3** and **D4** geometries, the position of Zn metal on BP causes shifting of a major part of HOMO on the metal center and LUMO on the cage end. This happens because of the presence of many electronegative atoms that make the metal atom electron-rich. A metal being electropositive cannot retain these electrons, and therefore, they are spread out as excess electrons causing high energy level of the newly formed HOMO. Moreover, in the **E1**−**E4** geometries, a similar distribution pattern of HOMO and LUMO densities is observed as shown in Figure 6.

2.6. Global Descriptor of Reactivity. The global descriptor of reactivity of investigated systems is inspected at the B3LYP/6-31G(d,p) level of DFT. Various properties such as global hardness (η), global softness (S), global ionization potential (IP), global electron affinity (EA), electrophilic index (ω), global chemical potential (μ), and electronegativity (χ) are carried out in order to illustrate the effect of Zn doping (Zn−BP) on the capturing of CO_2. The conventional energy of LUMO expresses the electron accepting property, whereas the energy of HOMO represents the IP (according to the Koopmann theorem[62]). The results in Table 3 reveal that all Zn-doped and CO_2-adsorbed Zn-decorated systems exhibit good affinity values with fine IP. The values of EA and IP suggested that our strategy of Zn decoration on pure $B_{12}P_{12}$ is useful for CO_2 adsorption. Similarly, the electrophilic index expresses the great chemical reactivity of a compound. The pure BP nanocage disclosed an electrophilic index of 6.703 eV. Fixing of Zn on $B_{12}P_{12}$ (**D1**−**D4**) boosted the electrophilic index value to 7.951 from 6.703 eV for bare nanocage. Likewise, adsorption of CO_2 on **D1**−**D4** geometries improved the electrophilic index values in **E1**−**E4** geometries, which recommended that Zn decoration is an effective way for CO_2 adsorption. Global hardness and global softness parameters also point out that Zn-decorated and CO_2-adsorbed Zn−BP nanocages are hard in nature with low values of global softness. The great chemical stability of a system is directly related to the chemical potential of that system. A compound with large value of chemical potential is supposed to be least reactive and most stable in nature. The Pure $B_{12}P_{12}$ nanocage exhibited a chemical potential value of −4.980 eV, whereas the positioning of Zn metal on the $B_{12}P_{12}$ nanocage increased the chemical potential in **D1** (μ(=−4.445 eV)), **D2** (μ(=−4.705 eV)), **D3**

https://dx.doi.org/10.1021/acsomega.0c01686
ACS Omega 2020, 5, 15547−15556

(μ(=−4.410 eV)), and **D4** (μ(=−4.370 eV)). Nonetheless, the adsorption of CO_2 on Zn-doped $B_{12}P_{12}$ nanocages (**E1**−**E4**) significantly raised the chemical potential. The decreasing order of chemical potential among **E1**−**E4** is [**E1** (μ(=−4.205 eV))] > [**E4** (μ(=−4.400 eV))] > [**E3** (μ(=−4.590 eV))] > [**E2** (μ(=−4.70 eV))]. Therefore, designed systems show good values of chemical potential and electronegativity. From the preceding discussion, it is concluded that all designed systems (Zn-decorated and CO_2-adsorbed $B_{12}P_{12}$ nanocages) exhibited ordinary reactivity with remarkable stability and thus proved to be the best candidates for CO_2 sensing materials.

3. CONCLUSIONS

In summary, the changes in the electronic behavior of $B_{12}P_{12}$ nanocage on Zn decoration and CO_2 adsorption are studied. Zn decoration on $B_{12}P_{12}$ followed by CO_2 adsorption on bare and Zn-decorated $B_{12}P_{12}$ causes narrowing of the HOMO−LUMO energy gap. The binding energy of CO_2-adsorbed Zn−$B_{12}P_{12}$ nanocages [**E1** (E_{ad} = −75.12 kJ/mol), **E2** (E_{ad} = −25.89 kJ/mol), **E3** (E_{ad} = −42.43 kJ/mol), and **E4** (E_{ad} = −28.73 kJ/mol)] is remarkably higher than those of Zn−$B_{12}P_{12}$ [**D1** (E_{ad} = −57.12 kJ/mol), **D2** (E_{ad} = −22.94 kJ/mol), **D3** (E_{ad} = −21.03 kJ/mol), and **D4** (E_{ad} = −14.07 kJ/mol)] systems, which suggested the strong adsorption of CO_2 on Zn-decorated BP systems. The dipole moment and Q_{NBO} analysis showed that maximum charge separation is observed for CO_2−Zn−$B_{12}P_{12}$ geometries. MEP analysis confirmed the different charge zones on all systems. DOS analysis is also performed in support of FMO analysis, which explored the different distribution patterns of HOMO and LUMO orbitals on CO_2-adsorbed and Zn-decorated $B_{12}P_{12}$ geometries. Finally, the global descriptors of reactivity are investigated, which demonstrated the great stability and least reactivity of our designed (Zn−$B_{12}P_{12}$ and CO_2−Zn−$B_{12}P_{12}$) systems. The results of all analyses recommended our Zn-decorated $B_{12}P_{12}$ nanocages as potential candidates for application in CO_2 sensors.

4. COMPUTATIONAL METHODS

The B3LYP method of DFT along with the 6-31G(d,p) basis set is utilized for performing all calculations through Gaussian 09.[63] The same level of DFT is used in order to gain optimized geometries of all systems of interest. B3LYP[64,65]/6-31G-(d,p)[66,67] is a reliable level of DFT for computing the geometric and electronic properties of nanocages[23,53,54] and other systems.[68,69] Different parameters such as adsorption energy, Q_{NBO}, dipole moment, analysis of MEP, FMO distribution, and DOS are estimated at the B3LYP/6-31G(d,p) level of DFT. The HOMO−LUMO gap is directly related to the conductivity of a material and also plays a key role in evaluating the global descriptor of reactivity. Global hardness, global softness, electronegativity, chemical potential, IP, EA, and electrophilic index of all systems are calculated by using HOMO−LUMO gap values. Different equations are used to calculate the interaction energies of CO_2 gas and Zn metal with $B_{12}P_{12}$ nanocages.

Equation 2 is useful for calculating the adsorption energy of the Zn−$B_{12}P_{12}$ system

$$E_{ad} = E_{Zn-BP} - (E_{BP} + E_{Zn}) \quad (2)$$

In this equation, E_{Zn-BP} stands for the zinc metal-decorated $B_{12}P_{12}$ nanocage. Similarly, E_{BP} expresses the energy of bare $B_{12}P_{12}$ nanocage and E_{Zn} points out the energy of Zn (metal). The adsorption energies in kJ/mol for CO_2-adsorbed pure and Zn-decorated $B_{12}P_{12}$ are calculated with the aid of eqs 3 and 4.

$$E_{int(BP)} = E_{CO_2-BP} - (E_{BP} + E_{CO_2}) \quad (3)$$

$$E_{int(Zn-BP)} = E_{CO_2-Zn-BP} - (E_{Zn-BP} + E_{CO_2}) \quad (4)$$

The $E_{int(BP)}$ in eq 2 and the $E_{int(Zn-BP)}$ in eq 4 define the interaction energies of CO_2 with pristine $B_{12}P_{12}$ and Zn-decorated $B_{12}P_{12}$, respectively. The E_{CO_2-BP} and $E_{CO_2-Zn-BP}$ fragments highlight the total interaction energies of the CO_2-adsorbed BP nanocage and CO_2-adsorbed Zn−BP nanocages, respectively. Similarly, E_{CO_2} indicates the single CO_2 molecule energy in kJ/mol.

Valuable literature suggests that different equations were utilized for calculating different global indices of reactivity [electrophilicity index (ω), global softness (S), electronegativity (X), global hardness (η), and chemical potential (μ)], which are given below[70,71]

$$\mu = -1/2 \times (E_{HOMO} + E_{LUMO}) \quad (5)$$

$$\eta = (E_{LUMO} - E_{HOMO})/2 \quad (6)$$

$$S = 1/(2\eta) \quad (7)$$

$$\omega = \mu^2/2\eta \quad (8)$$

$$X = -(E_{LUMO} + E_{HOMO})/2 \quad (9)$$

The visualization software utilized to study the different properties of investigated systems are GaussView 5.0 (used to manage the input files), Avogadro (for interpreting the HOMO and LUMO distribution), and Pymolyz (for DOS graphs).

■ ASSOCIATED CONTENT

Supporting Information

The Supporting Information is available free of charge at https://pubs.acs.org/doi/10.1021/acsomega.0c01686.

Cartesian coordinates of the optimized geometries (PDF)

■ AUTHOR INFORMATION

Corresponding Author

Khurshid Ayub − *Department of Chemistry, COMSATS University, Abbottabad 22060, Pakistan;* orcid.org/0000-0003-0990-1860; Phone: +92-992-383591-6; Email: khurshid@cuiatd.edu.pk; Fax: +92-992-383441

Authors

Shahid Hussain − *Department of Applied Chemistry, Government College University, Faisalabad 38000, Pakistan*

Shahzad Ali Shahid Chatha − *Department of Applied Chemistry, Government College University, Faisalabad 38000, Pakistan*

Abdullah Ijaz Hussain − *Department of Applied Chemistry, Government College University, Faisalabad 38000, Pakistan*

Riaz Hussain − *Department of Chemistry, University of Okara, Okara 56300, Punjab, Pakistan*

Muhammad Yasir Mehboob − *Department of Chemistry, University of Okara, Okara 56300, Punjab, Pakistan;* orcid.org/0000-0002-7143-1129

https://dx.doi.org/10.1021/acsomega.0c01686
ACS Omega 2020, 5, 15547−15556

Tahsin Gulzar − *Department of Applied Chemistry, Government College University, Faisalabad 38000, Pakistan*
Asim Mansha − *Department of Applied Chemistry, Government College University, Faisalabad 38000, Pakistan;* orcid.org/0000-0001-5659-0562
Nabeel Shahzad − *Department of Applied Chemistry, Government College University, Faisalabad 38000, Pakistan*

Complete contact information is available at: https://pubs.acs.org/10.1021/acsomega.0c01686

Notes

The authors declare no competing financial interest.

■ ACKNOWLEDGMENTS

The authors acknowledge the financial and technical support from Shakarganj Limited, Jhang, Punjab, Pakistan.

■ REFERENCES

(1) Murray, C. B.; Kagan, C. R.; Bawendi, M. G. Synthesis and Characterization of Monodisperse Nanocrystals and Close-Packed Nanocrystal Assemblies. *Annu. Rev. Mater. Sci.* **2000**, *30*, 545−610.
(2) Wu, H.-S.; Cui, X.-Y.; Qin, X.-F.; Strout, D. L.; Jiao, H. Boron Nitride Cages from B12N12 to B36N36: Square−hexagon Alternants vs Boron Nitride Tubes. *J. Mol. Model.* **2006**, *12*, 537−542.
(3) Li, J. L.; Hu, Z. S.; Yang, G. W. High-Capacity Hydrogen Storage of Magnesium-Decorated Boron Fullerene. *Chem. Phys.* **2012**, *392*, 16−20.
(4) Yin, B.; Wang, G.; Sa, N.; Huang, Y. Bonding Analysis and Stability on Alternant B16N16 Cage and Its Dimers. *J. Mol. Model.* **2008**, *14*, 789−795.
(5) Baei, M. T.; Peyghan, A. A.; Bagheri, Z. A DFT Study on CO_2 Interaction with a BN Nano-Cage. *Bull. Korean Chem. Soc.* **2012**, *33*, 3338−3342.
(6) Lee, S.-S.; Yee, K.-A.; Yi, H.-S.; Kang, S.-K.; Seong, S.-Y. The Electronic Structure and Stability of the Heterofullerene:C (60-2x) (BN) X. *Bull. Korean Chem. Soc.* **2003**, *24*, 494−498.
(7) Hadipour, N. L.; Ahmadi Peyghan, A.; Soleymanabadi, H. Theoretical Study on the Al-Doped ZnO Nanoclusters for CO Chemical Sensors. *J. Phys. Chem. C* **2015**, *119*, 6398−6404.
(8) Bachtold, A. Logic Circuits with Carbon Nanotube Transistors. *Science* **2001**, *294*, 1317−1320.
(9) Rad, A. S.; Ayub, K. Adsorption of Pyrrole on $Al_{12}N_{12}$, $Al_{12}P_{12}$, $B_{12}N_{12}$, and $B_{12}P_{12}$ Fullerene-like Nano-Cages; a First Principles Study. *Vacuum* **2016**, *131*, 135−141.
(10) Soltani, A.; Baei, M. T.; Taghartapeh, M. R.; Lemeski, E. T.; Shojaee, S. Phenol Interaction with Different Nano-Cages with and without an Electric Field: A DFT Study. *Struct. Chem.* **2015**, *26*, 685−693.
(11) Ullah, F.; Kosar, N.; Ali, A.; Maria; Mahmood, T.; Ayub, K. Alkaline Earth Metal Decorated Phosphide Nanoclusters for Potential Applications as High Performance NLO Materials; A First Principle Study. *Phys. E* **2020**, *118*, 113906.
(12) Ullah, F.; Kosar, N.; Ali, A.; Maria; Mahmood, T.; Ayub, K. Design of Novel Inorganic Alkaline Earth Metal Doped Aluminum Nitride Complexes (AEM@$Al_{12}N_{12}$) with High Chemical Stability, Improved Electronic Properties and Large Nonlinear Optical Response. *Optik* **2020**, *207*, 163792.
(13) Munsif, S.; Maria; Khan, S.; Ali, A.; Gilani, M. A.; Iqbal, J.; Ludwig, R.; Ayub, K. Remarkable Nonlinear Optical Response of Alkali Metal Doped Aluminum Phosphide and Boron Phosphide Nanoclusters. *J. Mol. Liq.* **2018**, *271*, 51−64.
(14) Kandalam, A. K.; Blanco, M. A.; Pandey, R. Theoretical Study of Al_nN_n , Ga_nN_n , and In_n N_n (n = 4, 5, 6) Clusters. *J. Phys. Chem. B* **2002**, *106*, 1945−1953.
(15) Costales, A.; Kandalam, A. K.; Franco, R.; Pandey, R. Theoretical Study of Structural and Vibrational Properties of $(AlP)_n$, $(AlAs)_n$, $(GaP)_n$, $(GaAs)_n$, $(InP)_n$, and $(InAs)_n$ Clusters with n = 1, 2, 3. *J. Phys. Chem. B* **2002**, *106*, 1940−1944.
(16) Yong, Y.; Liu, K.; Song, B.; He, P.; Wang, P.; Li, H. Coalescence of BnNn Fullerenes: A New Pathway to Produce Boron Nitride Nanotubes with Small Diameter. *Phys. Lett. A* **2012**, *376*, 1465−1467.
(17) Guldi, D. M.; Illescas, B. M.; Atienza, C. M.; Wielopolski, M.; Martín, N. Fullerene for Organic Electronics. *Chem. Soc. Rev.* **2009**, *38*, 1587.
(18) Beheshtian, J.; Kamfiroozi, M.; Bagheri, Z.; Ahmadi, A. Computational Study of CO and NO Adsorption on Magnesium Oxide Nanotubes. *Phys. E* **2011**, *44*, 546−549.
(19) Ayub, K. Binding Affinity and Permeation of $X_{12}Y_{12}$ Nanoclusters for Helium and Neon. *J. Mol. Liq.* **2017**, *244*, 124−134.
(20) Rad, A. S.; Ayub, K. DFT Study of Boron Trichloride Adsorption on the Surface of $Al_{12}N_{12}$ Nanocluster. *Mol. Phys.* **2017**, *115*, 879−884.
(21) Rad, A. S.; Ayub, K. Detailed Surface Study of Adsorbed Nickel on $Al_{12}N_{12}$ Nano-Cage. *Thin Solid Films* **2016**, *612*, 179−185.
(22) Baei, M. T.; Mohammadian, H.; Hashemian, S. $B_{12}N_{12}$ Nanocage as a Potential Adsorbent for the Removal of Aniline from Environmental Systems. *Bulg. Chem. Commun.* **2014**, *46*, 735−742.
(23) Baei, M. T. Remove of Toxic Pyridine from Environmental Systems by Using $B_{12}N_{12}$ Nano-Cage. *Superlattices Microstruct.* **2013**, *58*, 31−37.
(24) Esrafili, M. D.; Nurazar, R. Methylamine Adsorption and Decomposition on $B_{12}N_{12}$ Nanocage: A Density Functional Theory Study. *Surf. Sci.* **2014**, *626*, 44−48.
(25) Baei, M. T. $B_{12}N_{12}$ Sodalite like Cage as Potential Sensor for Hydrogen Cyanide. *Comput. Theor. Chem.* **2013**, *1024*, 28−33.
(26) Wang, H. Density Functional Investigation of Fluorinated $B_{12}N_{12}$ Clusters. *Chin. J. Chem.* **2010**, *28*, 1897−1901.
(27) Baei, M. T.; Taghartapeh, M. R.; Lemeski, E. T.; Soltani, A. A Computational Study of Adenine, Uracil, and Cytosine Adsorption upon AlN and BN Nano-Cages. *Phys. Rev. B: Condens. Matter Mater. Phys.* **2014**, *444*, 6−13.
(28) Rad, A. S.; Ayub, K. A Comparative Density Functional Theory Study of Guanine Chemisorption on $Al_{12}N_{12}$, $Al_{12}P_{12}$, $B_{12}N_{12}$, and $B_{12}P_{12}$ Nano-Cages. *J. Alloys Compd.* **2016**, *672*, 161−169.
(29) Rad, A. S. High Ozone Chemisorption by Using Metal−cluster Complexes: A DFT Study on the Nickel-Decorated $B_{12}P_{12}$ Nano-clusters. *Can. J. Chem.* **2017**, *95*, 845−850.
(30) Rad, A. S.; Ayub, K. How Can Nickel Decoration Affect H_2 Adsorption on $B_{12}P_{12}$ Nano-Heterostructures? *J. Mol. Liq.* **2018**, *255*, 168−175.
(31) Rad, A. S.; Abedini, E. Chemisorption of NO on Pt-Decorated Graphene as Modified Nanostructure Media: A First Principles Study. *Appl. Surf. Sci.* **2016**, *360*, 1041−1046.
(32) Rad, A. S. Adsorption of C_2H_2 and C_2H_4 on Pt-Decorated Graphene Nanostructure: Ab-Initio Study. *Synth. Met.* **2016**, *211*, 115−120.
(33) Rad, A. S.; Jouibary, Y. M.; Foukolaei, V. P.; Binaeian, E. Study on the Structure and Electronic Property of Adsorbed Guanine on Aluminum Doped Graphene: First Principles Calculations. *Curr. Appl. Phys.* **2016**, *16*, 527−533.
(34) Rad, A. S.; Foukolaei, V. P. Density Functional Study of Al-Doped Graphene Nanostructure towards Adsorption of CO, CO_2 and H_2O. *Synth. Met.* **2015**, *210*, 171−178.
(35) Rad, A. S. Al-Doped Graphene as a New Nanostructure Adsorbent for Some Halomethane Compounds: DFT Calculations. *Surf. Sci.* **2016**, *645*, 6−12.
(36) Arshad, Y.; Khan, S.; Hashmi, M. A.; Ayub, K. Transition Metal Doping: A New and Effective Approach for Remarkably High Nonlinear Optical Response in Aluminum Nitride Nanocages. *New J. Chem.* **2018**, *42*, 6976−6989.
(37) Gilani, M. A.; Tabassum, S.; Gul, U.; Mahmood, T.; Alharthi, A. I.; Alotaibi, M. A.; Geesi, M.; Sheikh, R.; Ayub, K. Copper-Doped $Al_{12}N_{12}$ Nano-Cages: Potential Candidates for Nonlinear Optical Materials. *Appl. Phys. A* **2018**, *124*, 14.

(38) Zhang, Y.; Zheng, X.; Zhang, S.; Huang, S.; Wang, P.; Tian, H. Bare and Ni Decorated $Al_{12}N_{12}$ Cage for Hydrogen Storage: A First-Principles Study. *Int. J. Hydrogen Energy* **2012**, *37*, 12411−12419.
(39) Rad, A. S.; Ayub, K. Enhancement in Hydrogen Molecule Adsorption on $B_{12}N_{12}$ Nano-Cluster by Decoration of Nickel. *Int. J. Hydrogen Energy* **2016**, *41*, 22182−22191.
(40) Rad, A. S.; Mirabi, A.; Peyravi, M.; Mirzaei, M. Nickel-Decorated $B_{12}P_{12}$ Nanoclusters as a Strong Adsorbent for SO_2 Adsorption: Quantum Chemical Calculations. *Can. J. Phys.* **2017**, *95*, 958−962.
(41) Rad, A. S.; Ayub, K. Adsorption Properties of Acetylene and Ethylene Molecules onto Pristine and Nickel-Decorated $Al_{12}N_{12}$ Nanoclusters. *Mater. Chem. Phys.* **2017**, *194*, 337−344.
(42) Shakerzadeh, E.; Khodayar, E.; Noorizadeh, S. Theoretical Assessment of Phosgene Adsorption Behavior onto Pristine, Al- and Ga-Doped $B_{12}N_{12}$ and $B_{16}N_{16}$ Nanoclusters. *Comput. Mater. Sci.* **2016**, *118*, 155−171.
(43) Ayub, K. Are Phosphide Nano-Cages Better than Nitride Nano-Cages? A Kinetic, Thermodynamic and Non-Linear Optical Properties Study of Alkali Metal Encapsulated $X_{12}Y_{12}$ Nano-Cages. *J. Mater. Chem. C* **2016**, *4*, 10919−10934.
(44) Maria; Iqbal, J.; Ayub, K. Enhanced Electronic and Non-Linear Optical Properties of Alkali Metal (Li, Na, K) Doped Boron Nitride Nano-Cages. *J. Alloys Compd.* **2016**, *687*, 976−983.
(45) Radosavljević, M.; Appenzeller, J.; Derycke, V.; Martel, R.; Avouris, P.; Loiseau, A.; Cochon, J.-L.; Pigache, D. Electrical Properties and Transport in Boron Nitride Nanotubes. *Appl. Phys. Lett.* **2003**, *82*, 4131−4133.
(46) Ayub, K. Transportation of Hydrogen Atom and Molecule through $X_{12}Y_{12}$ Nano-Cages. *Int. J. Hydrogen Energy* **2017**, *42*, 11439−11451.
(47) Tokoro, H.; Fujii, S.; Oku, T. Iron Nanoparticles Coated with Boron Nitride Nanolayers Synthesized by a Solid Phase Reaction. *IEEE Trans. Magn.* **2003**, *39*, 2761−2763.
(48) Zhuiykov, S.; Wlodarski, W.; Li, Y. Nanocrystalline V_2O_5−TiO_2 Thin-Films for Oxygen Sensing Prepared by Sol−gel Process. *Sens. Actuators, B* **2001**, *77*, 484−490.
(49) Chang, H.; Lee, J. D.; Lee, S. M.; Lee, Y. H. Adsorption of NH_3 and NO_2 Molecules on Carbon Nanotubes. *Appl. Phys. Lett.* **2001**, *79*, 3863−3865.
(50) Lu, J.; Nagase, S.; Maeda, Y.; Wakahara, T.; Nakahodo, T.; Akasaka, T.; Yu, D.; Gao, Z.; Han, R.; Ye, H. Adsorption Configuration of NH_3 on Single-Wall Carbon Nanotubes. *Chem. Phys. Lett.* **2005**, *405*, 90−92.
(51) Sedjo, R.; Sohngen, B. Carbon Sequestration in Forests and Soils. *Annu. Rev. Resour. Econ.* **2012**, *4*, 127−144.
(52) Holloway, S.; Pearce, J.; Hards, V.; Ohsumi, T.; Gale, J. Natural Emissions of CO_2 from the Geosphere and Their Bearing on the Geological Storage of Carbon Dioxide. *Energy* **2007**, *32*, 1194−1201.
(53) Hussain, S.; Hussain, R.; Mehboob, M. Y.; Chatha, S. A. S.; Hussain, A. I.; Umar, A.; Khan, M. U.; Ahmed, M.; Adnan, M.; Ayub, K. Adsorption of Phosgene Gas on Pristine and Copper-Decorated $B_{12}N_{12}$ Nanocages: A Comparative DFT Study. *ACS Omega* **2020**, *5*, 7641−7650.
(54) Hussain, S.; Chatha, S. A. S.; Hussain, A. I.; Hussain, R.; Mehboob, M. Y.; Muhammad, S.; Ahmad, Z.; Ayub, K. Zinc-Doped Boron Phosphide Nanocluster as Efficient Sensor for SO_2. *Acad. J. Chem.* **2020**, *2020*, 1−12.
(55) Kauffman, D. R.; Alfonso, D.; Matranga, C.; Qian, H.; Jin, R. Experimental and Computational Investigation of Au_{25} Clusters and CO_2: A Unique Interaction and Enhanced Electrocatalytic Activity. *J. Am. Chem. Soc.* **2012**, *134*, 10237−10243.
(56) Liang, X.; Zhang, Q.; Zhao, Q.; Zhao, H.; Feng, Y.; Suo, B.; Han, H.; Song, Q.; Li, Y.; Zou, W.; et al. CO_2 Adsorption on the $B_{12}N_{12}$ Nanocage Encapsulated with Alkali Metals: A Density Functional Study. *Nano* **2019**, *14*, 1950034.
(57) Jiang, Y.; Xie, X.; Hamid, I.; Chen, C.; Duan, H. Theoretical Simulation of CO_2 Capture by $Al_{11}Mg_3^-$ Cluster. *Mater. Res. Express* **2017**, *4*, 046302.
(58) Guo, H.; Zhang, W.; Lu, N.; Zhuo, Z.; Zeng, X. C.; Wu, X.; Yang, J. CO_2 Capture on h -BN Sheet with High Selectivity Controlled by External Electric Field. *J. Phys. Chem. C* **2015**, *119*, 6912−6917.
(59) Li, S. S. Scattering Mechanisms and Carrier Mobilities in Semiconductors. In *Semiconductor Physical Electronics*; Springer: New York, NY, 2006; pp 211−245
(60) Hussain, R.; Khan, M. U.; Mehboob, M. Y.; Khalid, M.; Iqbal, J.; Ayub, K.; Adnan, M.; Ahmed, M.; Atiq, K.; Mahmood, K. Enhancement in Photovoltaic Properties of N , N -diethylaniline Based Donor Materials by Bridging Core Modifications for Efficient Solar Cells. *ChemistrySelect* **2020**, *5*, 5022−5034.
(61) Afzal, Z.; Hussain, R.; Khan, M. U.; Khalid, M.; Iqbal, J.; Alvi, M. U.; Adnan, M.; Ahmed, M.; Mehboob, M. Y.; Hussain, M.; et al. Designing Indenothiophene-Based Acceptor Materials with Efficient Photovoltaic Parameters for Fullerene-Free Organic Solar Cells. *J. Mol. Model.* **2020**, *26*, 137.
(62) Koopmans, T. Ordering of Wave Functions and Eigenenergies to the Individual Electrons of an Atom. *Phys* **1933**, *1*, 104−113.
(63) Frisch, M. J.; Trucks, G. W.; Schlegel, H. B.; Scuseria, G. E.; Robb, M. A.; Cheeseman, J. R.; Scalmani, G.; Barone, V.; Mennucci, B.; Petersson, G. A.; Nakatsuji, H.; Caricato, M.; Li, X.; Hratchian, H. P.; Izmaylov, A. F.; Bloino, J.; Zheng, G.; Sonnenberg, J. L.; Hada, M.; Ehara, M.; Toyota, K.; Fukuda, R.; Hasegawa, J.; Ishida, M.; Nakajima, T.; Honda, Y.; Kitao, O.; Nakai, H.; Vreven, T.; Montgomery, J. A., Jr.; Peralta, J. E.; Ogliaro, F.; Bearpark, M.; Heyd, J. J.; Brothers, E.; Kudin, K. N.; Staroverov, V. N.; Kobayashi, R.; Normand, J.; Raghavachari, K.; Rendell, A.; Burant, J. C.; Iyengar, S. S.; Tomasi, J.; Cossi, M.; Rega, N.; Millam, J. M.; Klene, M.; Knox, J. E.; Cross, J. B.; Bakken, V.; Adamo, C.; Jaramillo, J.; Gomperts, R.; Stratmann, R. E.; Yazyev, O.; Austin, A. J.; Cammi, R.; Pomelli, C.; Ochterski, J. W.; Martin, R. L.; Morokuma, K.; Zakrzewski, V. G.; Voth, G. A.; Salvador, P.; Dannenberg, J. J.; Dapprich, S.; Daniels, A. D.; Farkas, Ö.; Foresman, J. B.; Ortiz, J. V.; Cioslowski, J.; Fox, D. J. *Gaussian 09, Revision C.01*; Gaussian, Inc.: Wallingford CT, 2013.
(64) Becke, A. D. Density-functional thermochemistry. III. The role of exact exchange. *J. Chem. Phys.* **1993**, *492*, 5648−5652.
(65) Lee, C.; Yang, W.; Parr, R. G. Density-Functional Exchange-Energy Approximation with Correct Asymptotic Behaviour. *Phys. Rev. B: Condens. Matter Mater. Phys.* **1988**, *37*, 785−789.
(66) Parr, R.; Hehre, W. J.; Pople, J. A. Self-Consistent Molecular-Orbital Methods. IX. An Extended Gaussian-Type Basis for Molecular-Orbital Studies of Organic Molecules. *J. Chem. Phys.* **1971**, *54*, 724−728.
(67) Hehre, W. J.; Ditchfield, R.; Pople, J. A. Self—Consistent Molecular Orbital Methods. XII. Further Extensions of Gaussian—Type Basis Sets for Use in Molecular Orbital Studies of Organic Molecules. *J. Chem. Phys.* **1972**, *56*, 2257−2261.
(68) Ashraf, A.; Carter-Fenk, K.; Herbert, J. M.; Farooqi, B. A.; Farooq, U.; Ayub, K. Interaction of Graphene Quantum Dots with Oligothiophene: A Comprehensive Theoretical Study. *J. Phys. Chem. C* **2019**, *123*, 29556−29570.
(69) Fazl-i-Sattar; Ahmed, A.; Ullah, H.; Ullah, Z.; Tariq, M.; Ayub, K. External Stimulus Controlled Recombination of Hydrogen in Photochromic Dithienylethene Frustrated Lewis Pairs. *Int. J. Hydrogen Energy* **2019**, *44*, 31141−31152.
(70) Parr, R. G.; Szentpály, L. v.; Liu, S. Electrophilicity Index. *J. Am. Chem. Soc.* **1999**, *121*, 1922−1924.
(71) Pearson, R. G. The Transition Metal-Carbon Monoxide Bond. *Inorg. Chem.* **1984**, *23*, 4675−4679.

https://dx.doi.org/10.1021/acsomega.0c01686
ACS Omega 2020, 5, 15547−15556